IAC-15.A6.9.5x29673

DETERMINING THE INFLUENCE ON ORBIT PREDICTION BASED ON UNCERTAINTIES IN ATMOSPHERIC MODELS

Christopher Kebschull[a], R. Ströbel[a], V. Braun[b], E. Stoll[a]

[a]*Institute of Space Systems, Technische Universität Braunschweig, Hermann-Blenk-Str. 23, 38108 Braunschweig, Germany*

[b]*Space Debris Office, ESA/ESOC, Robert-Bosch-Str. 5, 64293 Darmstadt, Germany*

Abstract

Orbit prediction and knowing its uncertainties is a key part in planning collision avoidance maneuvers or conducting re-entry estimations. For high accuracy forecasts numerical propagators are used. These propagators use force models to estimate the perturbing elements that affect a satellite's orbit. Especially on low Earth orbits (LEO) with decreasing perigee altitude the atmosphere becomes the dominating perturbing force. The available atmospheric models are complex in nature and react very sensitive to their input data. As with any model the atmospheric models also feature uncertainties. Because they heavily depend on the solar and geomagnetic activity, further uncertainty is introduced due to insufficient forecast capabilities of the solar and geomagnetic activity. The uncertainties introduced to the orbit prediction due to the atmospheric model's input parameters are investigated. The approach is to analyze the trajectory of different satellites, which are on different altitudes and inclinations. Using a numerical propagator a baseline is established applying observed solar and geomagnetic activity data of the past and estimate the satellites' orbit. Different types of solar and geomagnetic activity forecasts are used as implemented in the Orbital Spacecraft Active Removal (OSCAR) software, a tool of ESA's Debris Risk Assessment and Mitigation Analysis (DRAMA) software suite. The orbit prediction is repeated with the different solar and geomagnetic forecasts. The uncertainties of the orbit prediction as a result of the comparison to the baseline are shown.

Keywords: Numerical propagator, Orbit prediction, Uncertainty, Atmospheric model

I INTRODUCTION

The goal of this paper is to investigate the influence of uncertainties in atmospheric models based on solar activity forecasts on the orbit prediction errors. The model NRLMSISE-00 is considered for this. Because the model largely depends on the input of the solar and geomagnetic activity indices F10.7 and Ap, an impact on the orbit prediction is expected when varying these parameters. In order to get meaningful parameter sets as input for the prop-

Email address: c.kebschull@tu-braunschweig.de (Christopher Kebschull)

agation tool, different solar activity forecasts are generated using the **O**rbital **S**pace**C**raft **A**ctive **R**emoval (OSCAR) tool. OSCAR is part of ESA's **D**ebris **R**isk **A**ssessment and **M**itigation **A**nalysis (DRAMA) tool suite. For the propagation of the trajectory the **N**PI **E**phemeris **P**ropagation **T**ool and **UN**certainty **E**xtrapolation (NEPTUNE) is used. Both tools will be introduced in Sec. I.1 and I.2, respectively. The methodology of the simulations are explained in Sec. II, while the results are presented in Sec. II.1 and II.2. A conclusion and outlook is given in Sec. III.

I.1. OSCAR

The tool OSCAR has been re-developed in the scope of the recent DRAMA upgrade [9]. The software is capable of performing disposal maneuver analysis of space systems at the end of their mission. As part of the analysis OSCAR can determine an object's remaining orbital lifetime and check the compliance with established guidelines, such as the Space Debris Mitigation Guidelines of the UN COPUOS [2]. OSCAR is able to consider different disposal systems, e.g. chemical and electrical propulsion as well as electrodynamic tethers and drag augmentation systems [4]. For this paper, however, only the modeling of the future solar activity is used.

I.1.1. Solar Activity Forecast

Different approaches to predict the future solar activity exist. Because there has not been a consensus in the international community (yet) on which method is the most accurate and which method to use to verify the compliance with guidelines (several guidelines come with different recommended methods), five methods have been implemented in OSCAR:

- Latest Prediction,
- Best & Worst Case,
- Constant Solar Flux,
- ECSS Sample Solar Cycle,
- Monte Carlo Sampling.

The *Latest Prediction* is the only of the presented methods that takes into account data of the current solar cycle. This data is provided by ESOC/ESA as an update, which the user can download with a push of the button in the DRAMA graphical user interface. When the propagation timespan exceeds the available solar activity data, OSCAR will perform a forecast based on a modified McNish-Lincoln algorithm [10]. This approach is recommended in the ISO 27851 [3].
The *Best & Worst Case* forecast is also based on the Latest Prediction method. It is enhanced by an assumption of a confidence interval, which results in an upper and lower boundary. The lower boundary is being referred to as the Worst Case (WC). It corresponds to a longer orbital life time, while the upper boundary is called the Best Case (BC). For most objects it is associated with a shorter orbital lifetime of the object.
OSCAR also provides the user with the ability to disable any forecast of the solar activity. Values for an assumption of a *Equivalent Constant Solar Flux* can then be defined. This is the approach for LEO spacecraft in the French approach (STELA).
The so called *ECSS* method uses a simple approach to repeat the 23^{rd} solar cycle for the given timespan. This approach is recommended by the ECSS-E-ST-10-04C [1].
The fifth approach uses a *Monte Carlo* (MC) sampling algorithm. This is also recommended in the ISO 27852 [3]. For each day in the simulation the MC approach uses up to six past solar cycles. Detailed information on the forecasting methods implemented in OSCAR and on the DRAMA tool suite can be obtained in [5] and [8].

I.2. NEPTUNE

The second simulation tool, that has been used, is NEPTUNE. It has been developed at the Institute of Space Systems as part of ESA's **N**etwork **P**artnering **I**nitiative (NPI) program. NEPTUNE is a numerical propagator, which can be used for highly accurate orbit extrapolation purposes, like re-entry prediction or orbit determination. In the scope of this paper it is used to for a 30 day orbit prediction for a given object that is simulated to be on different orbits. Because the impact of uncertainties of the solar activity is analyzed, the modeling of perturbation forces is reduced to the atmospheric drag and the geopotential of degree 20 and order. As the geopotential model the EIGEN-GL04C (European Improved Gravity model of the Earth by New techniques) is used. NRLMSISE-00 is used for modeling the atmosphere. Its behavior is largely influenced by the solar and geomagnetic activity. Further information on NEPTUNE can be obtained in [6].

II SIMULATIONS

The simulations are performed in two parts. First OSCAR is used to forecast solar activity data for short periods of time of 30 days. Different methods are used to create different forecast results. The results are compared with measured F10.7 values of the same time period based on data supplied by ESA as part of the OSCAR software (*fap_day.dat & fap_mon.dat*). The time periods of low, medium and high solar activity have been considered. The maximum and medium values correspond to parts of the 23^{rd} solar cycle, while the minimum is chosen from the 24^{th} cycle, as shown in Fig. I:

- Minimum: 01.01.2009 - 30.01.2009,
- Medium: 01.06.2003 - 30.06.2003,
- Maximum: 01.03.2000 - 30.03.2000.

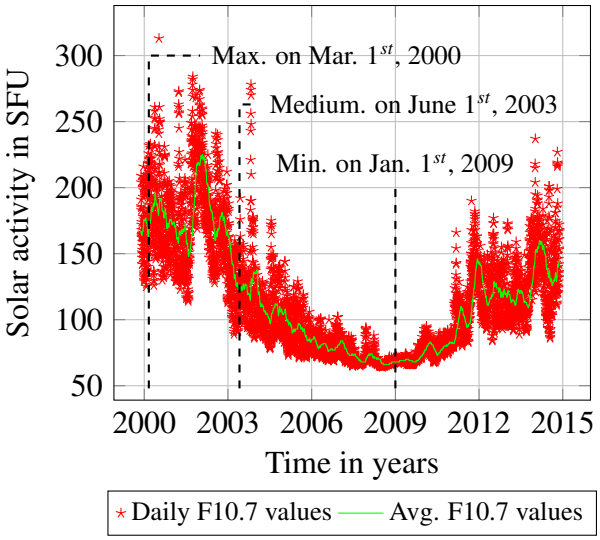

Fig. I: Chosen scenarios from the 23^{rd} and 24^{th} solar cycle.

Tab. I: Considered scenarios related to objects on different altitudes and inclination.

SMA [km]	Incl. [deg]	Orbit
6478	0.0°	Re-entering
6784	51.6°	ISS
6886	97.4°	TerraSAR-X
7144	98.4°	Envisat
7478	0.0°	High LEO

Different solar activity forecasts are used with NEPTUNE to propagate the trajectory of an object for 30 days in the second part. Different altitudes and inclinations have been chosen, based on a selection provided in [11]. Perfect circular orbits are assumed. Tab. I shows the scenarios.

In order to be able to compare the results of the scenarios the same object properties have been used in all simulations. These are listed in Tab. II.

II.1. Solar Activity Forecast

The first forecast over 30 days is performed for a time of low solar activity at the beginning of the 24^{th} solar cycle, from January 1^{st}, to January 30^{th}, 2009. The available version at the time of DRAMA (2.0.2), which contains

Tab. II: Object properties for all scenarios.

Property		Value
Mass	[kg]	2500.0
Cross section	[m^2]	10.0
Drag coefficient	[-]	2.2
Reflectivity coefficient	[-]	1.3

OSCAR 2.0.1 was used. The solar and geomagnetic activity data has been updated to May 18th, 2015, so that the chosen timeframes are well covered with measured data. All available methods have been chosen to create a forecast. The value of the confidence interval for the Best/Worst Case method has been left at its default setting (50%). The F10.7 value for the Constant Solar Flux method has been set to 70 solar flux units (SFU) and the Ap value to 5. These values are an assumption based on the values typical for this period of the solar cycle. The Monte Carlo Sampling factor has also been left at its default (2), so that the 22nd and 23rd solar cycles are used to derive a forecast for each day in the simulation. In comparison a Monte Carlo Sampling factor of 6 has also been used to show the impact of using the cycles 18 to 23.

The F10.7 results of the simulations are shown in Fig. II. The measured F10.7 values, as provided by the Latest Prediction method (and thus from the *fap_day.dat* provided by ESA), are shown as a black line (circle as mark). It moves between 68 and 72 SFU. All forecasting methods show almost constant results. The Best Case method moves between 70 and 72 SFU, while the Worst Case is at constant 67 SFU. The ECSS method shows an increased value of 74 SFU constantly. Higher discrepancies can be observed for the Monte Carlo Sampling methods. They moves between 66 and 98 SFU.

Fig. III shows the relative errors of all forecasting methods as compared to the measured values. The MC approaches show the highest deviation from the measured values of up to

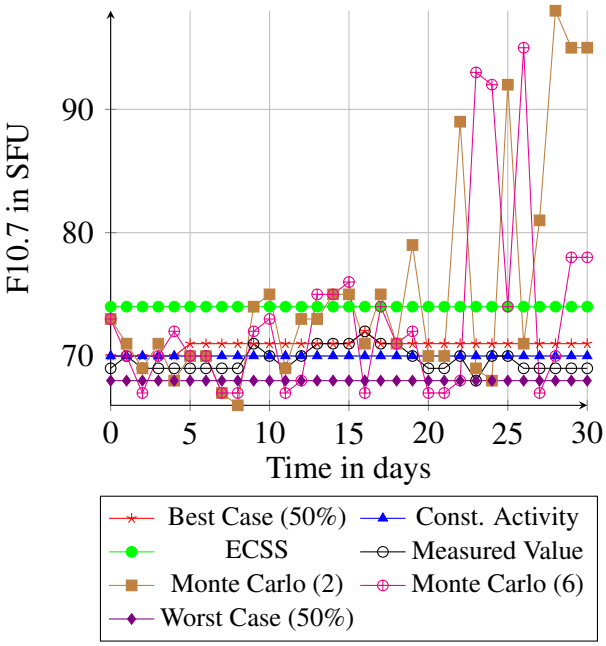

Fig. II: Prediction of the F10.7 values based on different forecasting methods for a time of low solar activity.

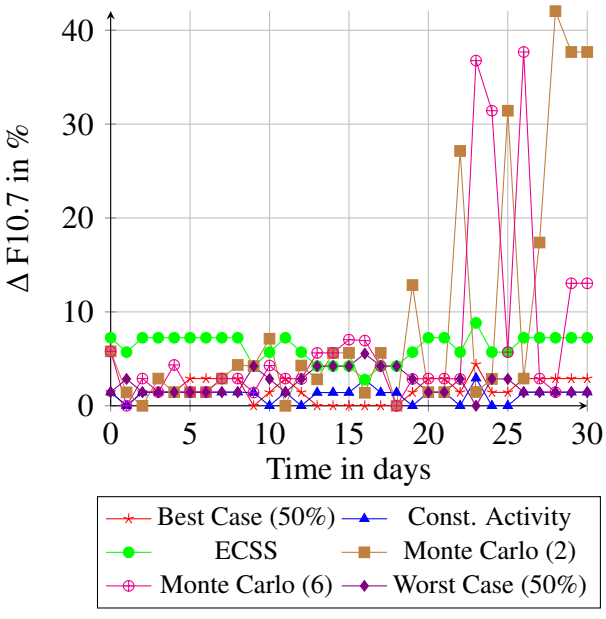

Fig. III: Relative prediction error of the F10.7 values based on different forecasting methods for a time of low solar activity.

40% for a given day. Increasing the sampling factor to 6 does not show a significant improvement over the default factor of 2. The other methods show a relative error below 10%. In this scenario, during a time of low solar activity, the Best Case and the assumption of a Constant Solar Flux of 70 SFU show the best results, with the lowest difference to the measured values (around 1% to 3% per day).
In the next 30 day forecast the Sun is in a state of medium activity. The forecast starts on the 1^{st} of June in 2003 and ends on the 30^{th} of that month. The settings are left the same except for the assumption of the Constant Solar Flux, which has been set to 135 SFU for the F10.7 and 10 respectively for the Ap index. The results in Fig. IV show a much higher fluctuation from about 91 to over 250 SFU. The measured values in these 30 days move between 105 and 192 SFU. The ECSS method and the Best Case results show an overall decreasing value from 184 to 179 SFU and 182 to 179 SFU. Because the Best Case depends on the results of the Latest Prediction it shows the spike to 192 SFU on day 10 in accordance with the measured value. The Worst Case results touch the lower end of the measured values. They move from 112 to 113 SFU while showing low peaks to 105 and 110 SFU at the points where the measured data decreases below the Worst Case estimate as well.

In Fig. V the relative deviation from the measured values are shown. Both MC Sampling methods show big relative errors of up to 166% per day. The ECSS method and the Best Case show the same behavior. Their errors range between 0% and up to 73%. The Worst Case shows a better performance with errors of 0% to 41%. The Constant Flux assumption shows the lowest variation with values between 0% and 29%.

For the scenario of high solar activity the timespan from March 1^{st} to March 30^{th}, 2000 is chosen. As the analysis for medium solar activity it is part of the 23^{rd} solar cycle. The

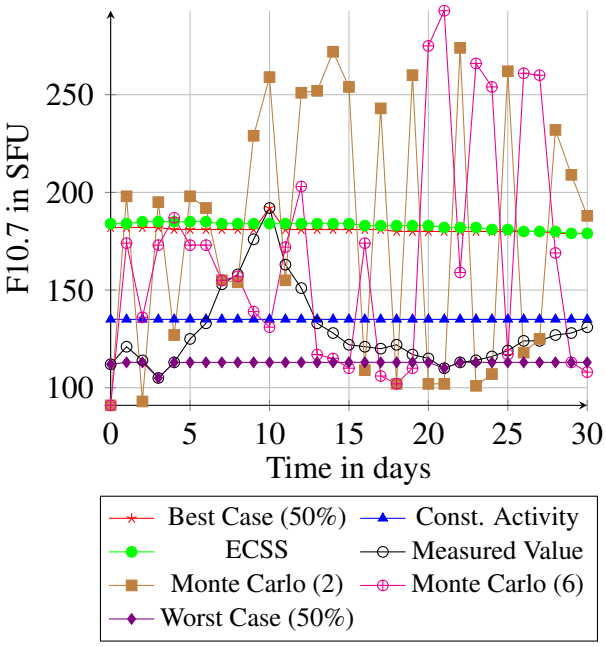

Fig. IV: Prediction of the F10.7 values based on different forecasting methods for a time of medium solar activity.

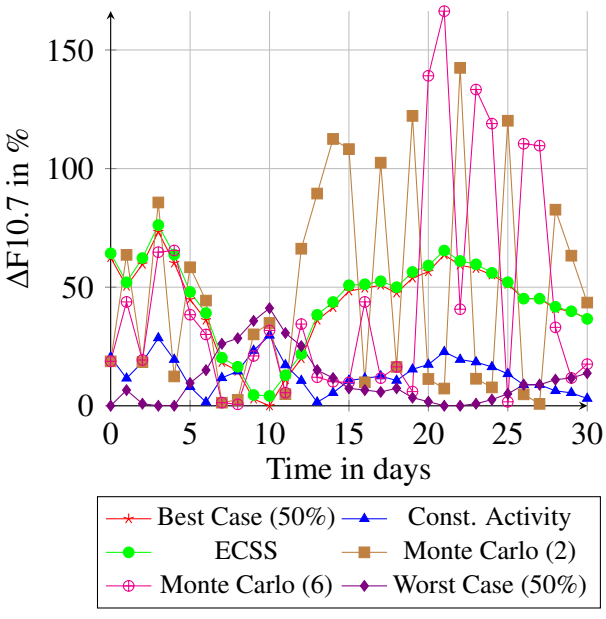

Fig. V: Relative prediction error of the F10.7 values based on different forecasting methods for a time of medium solar activity.

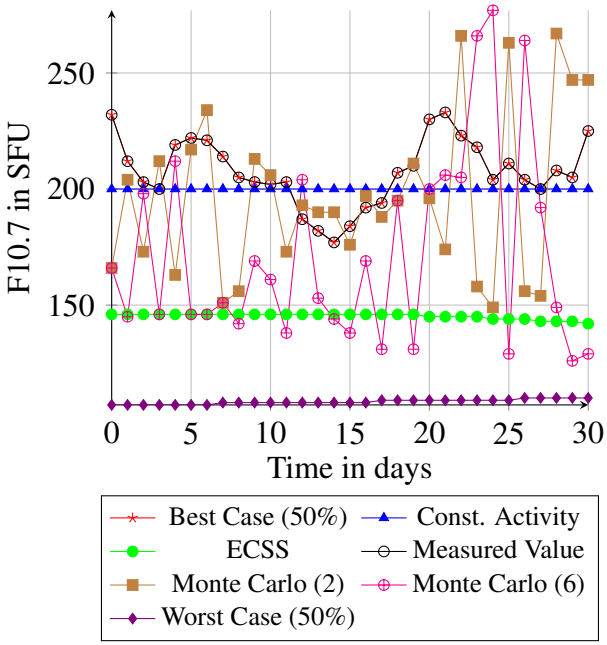

Fig. VI: Prediction of the F10.7 values based on different forecasting methods for a time of high solar activity.

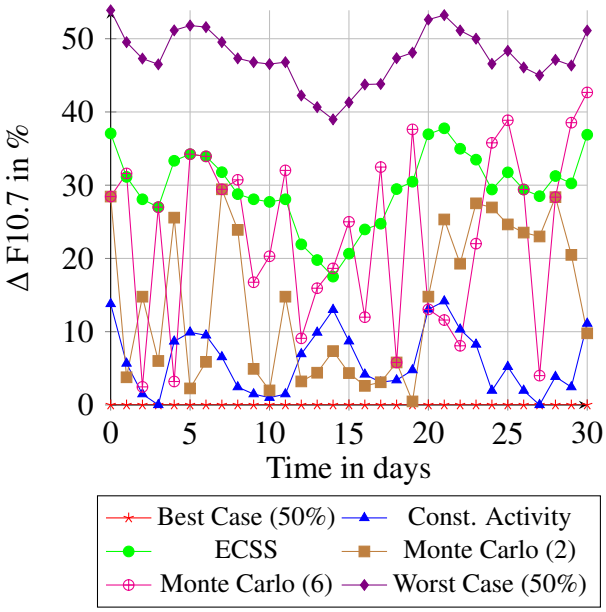

Fig. VII: Relative prediction error of the F10.7 values based on different forecasting methods for a time of high solar activity.

same settings are chosen for the forecasting methods, as before. The assumption however for the Constant Solar Flux is set to 200 SFU for the F10.7 and 15 for the Ap index. Fig. VI the resulting absolute values of the forecast are shown. It can be observed that the measured values are moving between 177 and 232 SFU. The results of the Best Case forecast is identical to the measured values. This means that the measured values are outside the upper bound of the 50% confidence interval, as the values of the Lastest Predictions (and thus the measured values) are assumed. The ECSS Sampling method shows a steady decline from 146 to 142 SFU, which is about 60 SFU lower than the average measured value (204.5 SFU). The Worst Case results move from 107 to 110 SFU and are far below the measured values. Both MC forecasts show high variations per day, ranging from 126 to 277 SFU.

Fig. VII shows that despite the high variations in the results of the forecasts the Monte Carlo Sampling methods perform better than the Worst Case. The MC relative deviations range from 0.5% up to 42% per day, while the Worst Case starts from 38% deviation to the highest value of 53%. The ECSS method moves between 17% and 37% relative error. The Constant Solar Flux assumption of 200 SFU produces a relative error of up to 14%. Because the Best Case forecast is in line with the measured values a 0% deviation can be observed. Again this is a case where the measured values would be above the upper bound for the 50% confidence interval. In order to prevent to show the results of the Latest Prediction method outside the Best Case/Worst Case interval the Best Case values assume the values of the Latest Prediction, which in this case are the actual measured values. Tab. III summarizes the results.

II.2. Orbit Prediction

As the next step in the analysis the different forecast results for the three different timespans are used to predict the orbit of the given objects

Tab. III: Summary of the simulation results for each forecasting method.

Solar Activity	Const.	Best Case	Worst Case	ECSS	MC (2)	MC (6)
Low	1% - 3%	0% - 4%	0% - 4%	1% - 9%	0% - 42%	1% - 37%
Medium	1% - 29%	0% - 73%	0% - 41%	5% - 76%	1% - 142%	0% - 166%
High	1% - 14%	0%	38% - 53%	19% - 37%	0% - 29%	2% - 42%

over the period of 30 days. For each object and each time period a trajectory is generated using measured solar activity data as input with the numerical propagator NEPTUNE. It is based on the orbits and object properties given in Tab. I and Tab. II respectively. As described in the previous section the other forecast methods introduce deviations in the solar activity values compared to the reference (measured values). Using this data further in the orbit prediction process will result in different trajectories and thus errors in the prediction. Theses errors are expressed in the satellite-centered UVW System [7], where the error of the orbit propagation using the forecasted solar activity is compared against the baseline trajectory, that has been generated with 0% error in the solar activity data. The transformation is started by defining:

$$\vec{U} = \frac{\vec{r}}{\left\|\vec{r}\right\|}, \quad \vec{W} = \frac{\vec{r}\times\vec{v}}{\left\|\vec{r}\times\vec{v}\right\|}, \quad \vec{V} = U \times W, \quad (1)$$

where U is referred to as the radial component. V is the along-track and W is the cross-track component. These are combined into the R matrix:

$$R = \begin{pmatrix} U_x & V_x & W_x \\ U_y & V_y & W_y \\ U_z & V_z & W_z \end{pmatrix}. \quad (2)$$

Applying this matrix on the baseline and the erroneous trajectory, which are available in earth-centered inertial (ECI) XYZ-coordinates, the UVW coordinates can be derived:

$$\begin{pmatrix} r_U \\ r_V \\ r_W \end{pmatrix} = R^{-1} \cdot \begin{pmatrix} X \\ Y \\ Z \end{pmatrix}. \quad (3)$$

Now the difference between both trajectories can be expressed in the satellite-centered coordinates:

$$\begin{pmatrix} \Delta r_U \\ \Delta r_V \\ \Delta r_W \end{pmatrix} = \begin{pmatrix} r_{U_0} \\ r_{V_0} \\ r_{W_0} \end{pmatrix} - \begin{pmatrix} r_U \\ r_V \\ r_W \end{pmatrix}, \quad (4)$$

where the baseline coordinates are marked with the 0-index. The previously introduced objects reside on different altitudes and inclinations. They have to be treated individually. In the following only the object on a 515 km altitude in a timespan of high solar activity is shown.

II.2.1. 515 km Orbit Scenarios

The trajectory of the object on a perfectly circular orbit at 515 km altitude and 51.6° inclination is propagated using NEPTUNE and the different solar activity data. Fig. VIII to X show the deviation of the predicted trajectory from the baseline. It is visible in all three figures that the scenarios using the ECSS and Monte Carlo Sampling methods lead to high deviations from the baseline trajectory. In radial (U) direction this leads to deviations of up to 150 m after 30 days, as shown in Fig. VII. Orbit predictions based on the results of the other methods stay below an error of 50 m.

Fig. IX shows the error in along-track (V) direction. This error is naturally greater due to errors in the radial direction, which has an influence on the orbital period of the object and typically causes a *leading ahead* or *trailing behind* behavior in relation to the baseline. As in the previous scenarios the greatest errors are introduced by results from the ECSS and the

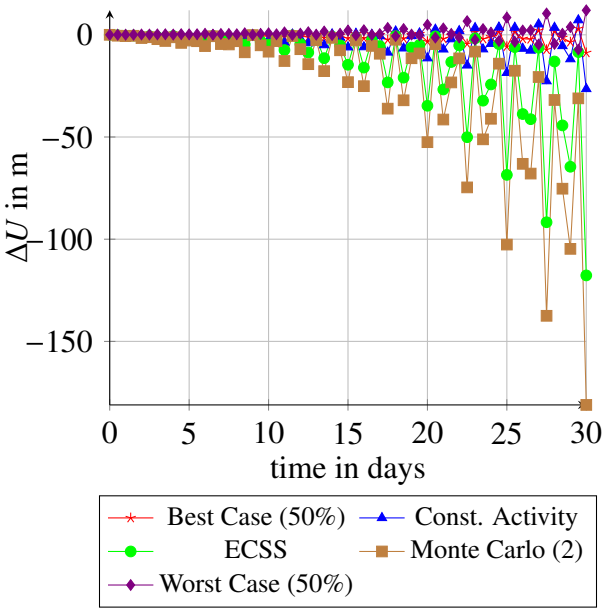

Fig. VIII: Difference in ΔU direction for an object in 515 km altitude at minimum solar activity.

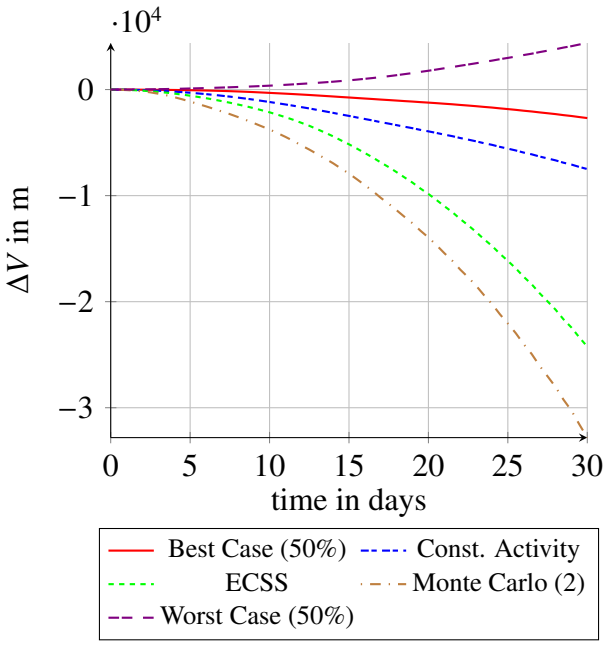

Fig. IX: Difference in ΔV direction for an object in 515 km altitude at minimum solar activity.

Monte Carlo Sampling methods leading to errors of up to -24.2 km and -32.8 km respectively. The lowest error is produced based on the forecast of the Best Case method. It has a deviation of -2.7 km after 30 days. The Constant Solar Flux method and the Worst Case both lead to errors of about -7.5 km and 7.0 km.

Looking at the cross-track (W) direction in Fig. X the errors are even an order of a magnitude smaller than in the radial direction. It is observable that the error increases periodically. The highest amplitudes are again produced by predictions using the ECSS and Monte Carlo Sampling methods, which are at about 5.0 m and 6.8 m respectively after 29.5 days. Using the results of the other methods causes an $|error| < 2\ m$ after 30 days. For a better analysis of this periodic behavior a finer data resolution is needed.

II.3. Uncertainty Analyses

To get an idea on how the error in the state vector scales with the error in the solar activ-

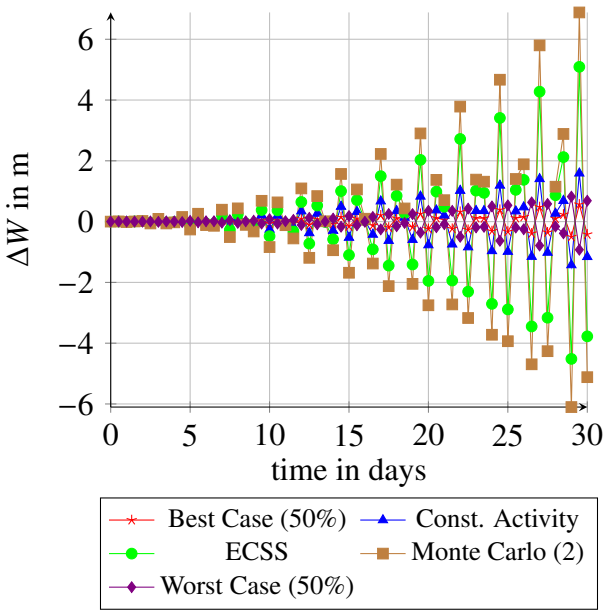

Fig. X: Difference in ΔW direction for an object in 515 km altitude at minimum solar activity.

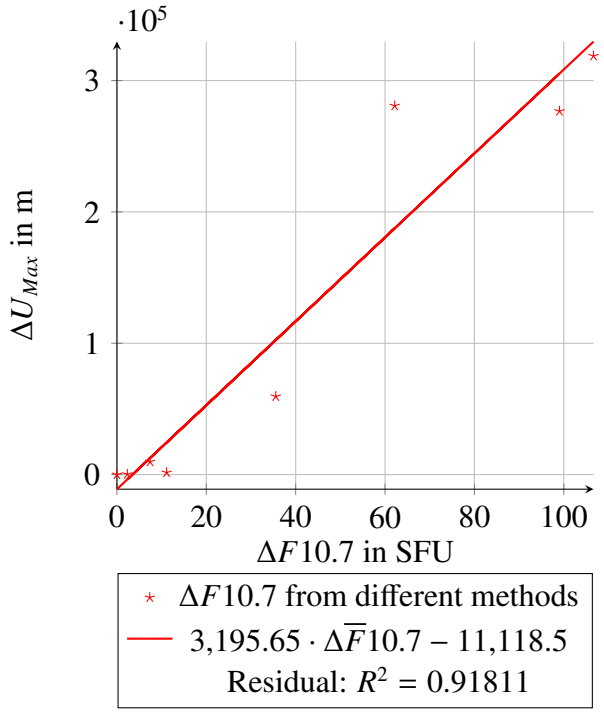

Fig. XI: Difference in U direction for an object in 515 km altitude.

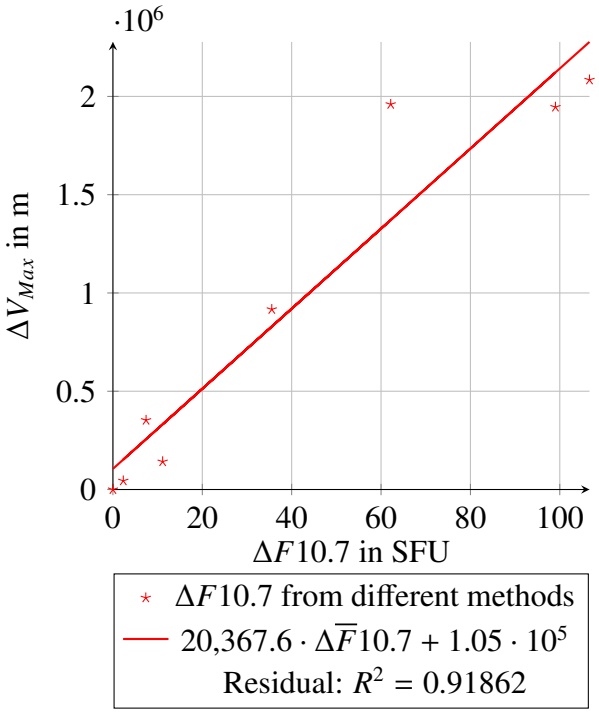

Fig. XII: Difference in V direction for an object in 515 km altitude.

ity forecast, the 515 km scenario has been further analyzed. A trend is derived using a linear regression as shown in Fig. XI to Fig. XIII for the radial, along-track and cross-track direction. The diagrams depict that a higher deviation in the solar activity data results in a higher deviation in the state vector of an object. It is also visible that the fit is not perfect. Because of the periodic nature of the increase of the error components and the rather low resolution of the data series it is not guaranteed that the considered values are the local maxima in each period. This can cause the variance in the diagrams. In addition the gravitational potential modeling is enabled in the orbit prediction simulation. Each trajectory might have a different gravity perturbation force because of the non-homogeneity of the Earth's mass, which is causing an additional impact on the variance seen in the diagrams.

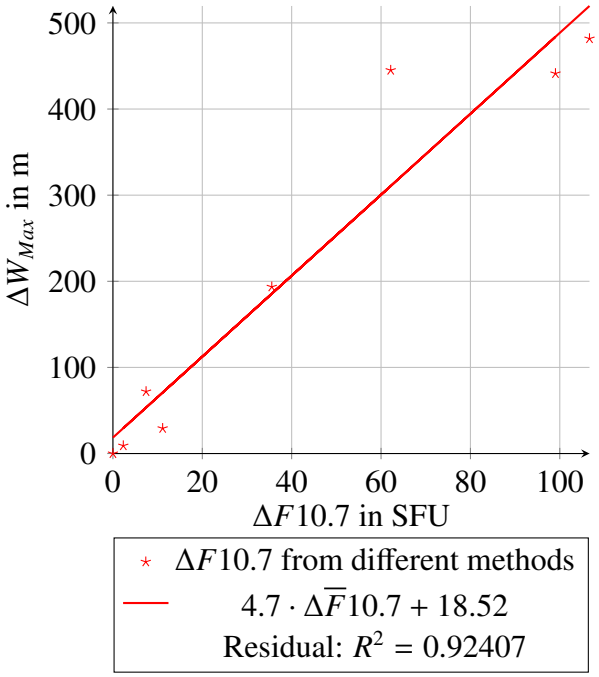

Fig. XIII: Difference in W direction for an object in 515 km altitude.

III CONCLUSION

Two separate analyses have been performed in this paper. Firstly the forecasting capabilities of the OSCAR tool have been evaluated for short timeframes up to 30 days for three different points in the solar cycle. Building up on these results in the second part, orbit prediction simulations with different forecasts of solar activity data have been performed using NEPTUNE as the numeric propagation tool. The results in each part have been compared to either the measured values of the solar activity or the baseline trajectory of a reference object. For the solar activity forecast it can be observed that the Best Case and the Constant Solar Flux assumption yield the best results for this forecast timeframe of 30 days. Of course such a short timespan is not the main field of operations for OSCAR, which was designed to cover simulation periods up to 200 years. However, the performed analysis shows which of the forecasting methods might also be applied for short timeframes.

For the orbit prediction part of the analysis all the solar activity forecasts of different quality have been used as input for the NEPTUNE propagation tool. The resulting trajectories of the same object have been compared with a baseline trajectory, which has been derived using a 0% variation in the solar activity. From this a linear trend between the errors in the solar activity prediction and the error in the orbit prediction can be observed. Higher deviations of the solar activity data (F10.7 values) lead to a higher deviation in the radial, along-track and cross-track components in the satellite-centered coordinate system. One example of an object on a 515 km orbit has been shown in this paper. Additional simulations have been performed for different orbits in the chosen solar activity scenarios. Future publications will contain a detailed statistical analysis. This analysis marks a starting point for a more complex and exhausting sensitivity analysis in which the F10.7 and Ap index will be varied directly in small increments. Additionally, the data resolution will be increased to be able to represent the periodicity that is part of the error growth shown in the satellite-centered coordinate system. This means that not only the time resolution is increased but also the orbit parameter bins are defined, e.g. it is envisaged to use smaller bins for objects on lower altitudes as compared to objects on higher altitudes, where it is sufficient to have bins covering several 100 km altitude. Parameters like the eccentricity and the right ascension of the ascending node will also be considered in the continuation of this analysis.

IV REFERENCES

[1] Anon. *Space engineering (Space environment)*, November 2008.

[2] Anon. *Space Debris Mitigation Guidelines of the Committee on the Peaceful Uses of Outer Space*. UN Office for Outer Space Affairs, 2010.

[3] Anon. *ISO27852:2011 Space systems - Estimation of orbit lifetime*, 2011.

[4] V. Braun, S. Flegel, J. Gelhaus, M. Möckel, C. Kebschull, J. Radtke, C. Wiedemann, and H. Krag. Orbital lifetime estimation using esa's oscar tool. In *Proceedings of the 5th European Conference for Aerospace Sciences*, 2013.

[5] V. Braun, S. Flegel, J. Gelhaus, M. Möckel, C. Kebschull, C. Wiedemann, N. Sanchez-Ortiz, H. Krag, and P. Vörsmann. Impact of solar flux modeling on satellite lifetime predictions. In *Proceedings of the 63rd International Astronauitcal Congress*, number IAC-12.A6.4.10, October 2012.

[6] V. Braun and A. Horstmann. Technical report - networking/partnering initiative tu-bs/esoc (2011 - 2015). Technical report, Insitute of Space Systems, 2015.

[7] T. Flohrer, H. Krag, and H. Klinkrad. Assessment and categorization of tle orbit errors for the us ssn catalogue. In *Proceedings of the Advanced Maui Optical and Space Surveillance Technologies Conference*, September 2008.

[8] J. Gelhaus, C. Kebschull, V. Braun, N. Sánchez-Ortiz, E. P. Endrino, J. M. Correia de Oliveira, and R. D. González. Drama final report - upgrade of esa's space debris mitigation analysis tool suite. Technical report, Institute of Aerospace Systems / DEIMOS Space S.L.U., July 2014.

[9] J. Gelhaus, N. Sánchez-Ortiz, V. Braun, C. Kebschull, J. Correia de Oliveira, R. Domínguez-González, C. Wiedemann, H. Krag, and P. Vörsmann. Upgrade of drama esa's space debris mitigation analysis tool suite. In *6th European Conference on Space Debris*, 2013.

[10] K. O. Niehuss, H. C. Euler Jr., and W. W. Vaughan. Statistical technique for intermediate and long-range estimation of 13-month smoothed solar flux and geomagnetic index. Technical report, NASA, 1996.

[11] R. Ströbel. Einfluss von ungenauigkeiten in atmosphärenmodellen auf die bahnvorhersage. Studienarbeit, TU Braunschweig, Institut für Luft- und Raumfahrtsysteme, Juni 2015.